Supporting Information

Spin crossover and structural phase transition in homochiral and heterochiral $Fe[(pybox)_2]^{2+}$ complexes

Wan-Qing Gao,‡[a] Yin-Shan Meng,‡[b] Chun-Hua Liu,[a] Yao Pan,[a] Tao Liu*[b] and Yuan-Yuan Zhu*[a,b]

*E-mail: yyzhu@hfut.edu.cn; liutao@dlut.edu.cn

[a]*School of Chemistry and Chemical Engineering, Hefei University of Technology and Anhui Key Laboratory of Advanced Functional Materials and Devices, Hefei 230009, China.*

[b]*State Key Laboratory of Fine Chemicals, Dalian University of Technology, 2 Linggong Road, Dalian 116024, China.*

Table of Contents

SI1 Instruments and Materials

SI1.1 Instruments

Structural characterization measurements. The NMR spectra were recorded on a Bruker 600 MHz spectrometer. FT-IR spectra were recorded on a Perkin-Elmer Spectrum BX FT-IR system using KBr pellets. Circular dichroism spectra were obtained by using a JASCO J1500 spectropolarimeter. Elemental analyses were measured using an Elementar Vario EL CUBE analyzer.

Magnetic properties measurements. Magnetic susceptibility data were collected using a Quantum Design MPMS XL-5 or PPMS-9T (EC-II) SQUID magnetometer. Measurements for all the samples were performed on microcrystalline powder restrained by a parafilm and loaded in a capsule. The magnetic susceptibility data were corrected for the diamagnetism of the samples using Pascal constants[53] and the sample holder and parafilm by corrected measurement.

X-ray Data Collection and Structure Determinations. Crystals suitable for single crystal X-ray diffraction were covered in a thin layer of hydrocarbon oil, mounted on a glass fiber attached to a copper pin, and placed under an N_2 cold stream. All data were carried out on a Rigaku Saturn724+ CCD diffractometer with Confocal-monochromator Mo-Kα radiation (λ = 0.71073 Å). Intensities were collected using CrystalClear (Rigaku Inc., 2008) technique and absorption corrections were applied using the 'multi-scan' method. Unit cell dimensions were obtained with least-squares refinements and all structures were solved by shelXT using olex2-1.2. The other nonhydrogen atoms were in successive difference Fourier syntheses. The final refinement was performed using full-matrix least-squares methods with anisotropic thermal parameters for non-hydrogen atoms on F_2. The hydrogen atoms were added theoretically and riding on the concerned atoms. Powder X-ray diffraction (PXRD) data for solvated samples were collected on Bruker D8 Venture diffractometer using a Cu $K\alpha$ radiation source (λ = 1.54178 Å) in the range of $5° < 2\theta < 50°$ at ambient temperature. Powder X-ray diffraction (PXRD) data for desolvated samples were performed on a Rigaku Dmax 2000 diffractometer with Cu $K\alpha$ radiation (λ = 1.54178 Å) in a flat plate geometry.

SI1.2 Materials

Enantiopure ligands 2,6-*bis*((*R* or *S*)-4-phenyl-4,5-dihydrooxazol-2-yl)pyridine ($\mathbf{L}^{\boldsymbol{R}}$ and $\mathbf{L}^{\boldsymbol{S}}$) were synthesized according to the literature procedures.[1] All other reagents and solvents were purchased commercially and used as supplied, unless otherwise stated.

Caution! Although not encountered in our experiments, perchlorate salts in the presence of organic ligands are potentially explosive. Only a small amount of the materials should be prepared and handled with care.

SI2 Synthesis and Structural Determination of Fe(II) Complexes

SI2.1 Synthesis of Fe(II) complexes

Synthesis of (*S*)-1·3MeCN. To a methanol solution (3 mL) of $\mathbf{L}^{S}$ (74 mg, 0.2 mmol) was added a methanol solution (3 mL) of $Fe(ClO_4)_2 \cdot 6H_2O$ (36 mg, 0.1 mmol) under stirring, the color of solution turn to dark violet immediately and precipitate was formed gradually. After stirring for about 1 hour, the precipitate was filtered and dried under vacuum. The precipitate was dissolved in MeCN (5 mL) and Et_2O (about 10 mL) was allowed to vapor diffuse into the solution during the period of three days. Dark violet cubic crystals (74 mg, 71%), suitable for X-ray crystallographic analysis, were obtained. ^{1}H NMR (600 MHz, CD_3CN): δ −3.1 (8 H), 3.3 (8 H) (Ph $H^{2/6}$+ $H^{3/5}$), 4.7 (4 H), 4.9 (4 H) (Ox H^3 and Ph H^4), 17.6 (4 H, Ox H^3), 25.1 (2 H, Py H^4), 30.1 (4 H, Ox H^4), 56.9 (4 H, Py $H^{3/5}$). IR (KBr plate): ν = 3627 (w), 3086 (w), 2940 (w), 2250 (w), 2015 (w), 1834 (w), 1642 (w), 1602 (w), 1575 (m), 1499 (m), 1457 (w), 1442 (w), 1405 (m), 1336 (w), 1276 (w), 1207 (w), 1146 (w), 1096 (s), 1030 (w), 1004 (w), 977 (w), 965 (w), 933 (m), 856 (w), 820 (w), 777 (w), 748 (w), 705 (w), 667 (w), 624 (m). Anal. Calcd for $C_{104}H_{94}Cl_4Fe_2N_{18}O_{24}$: C, 55.93; H, 4.24; N, 11.29. Found: C, 55.57; H, 4.52; N, 10.70.

Synthesis of (*rac*)-1·3MeCN. To a methanol solution (3 mL) of $\mathbf{L}^{R}$ (37 mg, 0.1 mmol) and $\mathbf{L}^{S}$ (37 mg, 0.1 mmol) was added a methanol solution (3 mL) of $Fe(ClO_4)_2 \cdot 6H_2O$ (36 mg, 0.1 mmol) under stirring. The following procedure is identical to that of **(*S*)-1·3MeCN**. Dark violet block crystals (87 mg, 78%), suitable for X-ray crystallographic analysis, were obtained. ^{1}H NMR (600 MHz, CD_3CN): δ 3.3 (8 H), 6.8 (8 H) (Ph $H^{2/6}$ + $H^{3/5}$), 4.6 (4 H), 6.2 (4 H), 7.2 (4 H), 7.6 (4 H) (Ox H^3 + H^4 and Ph H^4), 21.7 (2 H, Py H^4), 41.7 (4 H, Py $H^{3/5}$). IR (KBr plate): ν 3658 (w), 3084 (w), 2987 (w), 2258 (w), 1604 (w), 1576 (w), 1469 (w), 1458 (w), 1442 (w), 1404 (m), 1434 (w), 1259 (w), 1209 (w), 1076 (s), 974 (m), 960 (m), 935 (m), 862 (w), 814 (w), 775 (w), 746 (m), 706 (m), 667 (m), 621 (m), 588 (w), 567 (m). Anal. Calcd for $C_{52}H_{47}Cl_2FeN_9O_{12}$: C, 55.93; H, 4.24; N, 11.29. Found: C, 55.42; H, 4.29; N, 10.87.

Synthesis of (*S*)-2·$MeNO_2$. To a methanol solution (3 mL) of $\mathbf{L}^{S}$ (74 mg, 0.2 mmol) was added a methanol solution (3 mL) of $FeCl_2 \cdot 4H_2O$ (20 mg, 0.1 mmol) and $NaBPh_4$ (68 mg, 0.2 mmol) under stirring, the color of solution turn to dark violet immediately and precipitate was formed gradually. After stirring for about 1 hour, the precipitate was filtered and dried under vacuum. The precipitate was dissolved in nitromethane (5 mL) and Et_2O (about 10 mL) was allowed to vapor diffuse into the solution during the period of three days. Dark violet block crystals (102 mg, 68%), suitable for X-ray crystallographic analysis, were obtained. ^{1}H NMR (600 MHz, CD_3CN): δ −3.2 (8 H), 3.3 (8 H) (Ph $H^{2/6}$+ $H^{3/5}$), 4.7 (4 H), 4.9 (4 H) (Ox H^3 and Ph H^4), 6.9 (8 H), 7.1 (16 H), 7.4 (16 H) (BPh_4 H^4 +$H^{3/5}$+$H^{2/6}$), 17.7 (4 H, Ox H^3), 25.2 (2 H, Py H^4), 30.2 (4 H, Ox H^4), 57.3 (4 H, Py $H^{3/5}$). IR (KBr plate): ν = 3419 (w), 3054 (w), 3033 (w), 2983 (w), 2898 (w), 1954 (w), 1885 (w), 1638 (w), 1619 (w), 1572 (w), 1495 (w), 1480 (w), 1455 (w), 1425 (w), 1397 (w), 1324 (w), 1290 (w), 1276 (w), 1261 (w), 1200 (w), 1150 (w), 1135 (w), 1076 (w), 1031 (w), 972 (w), 927 (w), 943 (w), 771 (w),

747 (w), 734 (w), 704 (m), 612 (w), 553 (w), 514 (w), 470 (w), 435 (w). Anal. Calcd for $C_{95}H_{81}B_2FeN_7O_6$: C, 76.36; H, 5.46; N, 6.56. Found: C, 76.88; H, 5.62; N, 6.59.

Synthesis of (*rac*)-2·4MeNO$_2$. To a methanol solution (3 mL) of $\mathbf{L}^{\boldsymbol{S}}$ (74 mg, 0.2 mmol) was added a methanol solution (3 mL) of $FeCl_2 \cdot 4H_2O$ (20 mg, 0.1 mmol) and $NaBPh_4$ (68 mg, 0.2 mmol) under stirring. The following procedure is identical to that of **(*rac*)-1·MeCN**. Dark violet block crystals (87 mg, 78%), suitable for X-ray crystallographic analysis, were obtained. ^{1}H NMR (600 MHz, CD_3CN): δ 3.3 (8 H), 6.9 (8 H) (Ph $H^{2/6}$ + $H^{3/5}$), 4.5 (4 H), 6.3 (4 H), 7.2 (4 H), 7.6 (4 H) (Ox H^3 + H^4 and Ph H^4), 6.9 (8 H) ,7.0 (16 H), 7.3 (16 H) (BPh_4 H^4+$H^{3/5}$+$H^{2/6}$), 21.8 (2 H, Py H^4), 42.1 (4H, Py $H^{3/5}$). FT-IR (KBr plate): ν 3685 (w), 3057 (w), 2987 (w), 1639 (w), 1622 (w), 1574 (m), 1496 (w), 1481 (w), 1456 (w), 1425 (w), 1396 (m), 1288 (w), 1275 (w), 1250 (w), 1203 (m), 1078 (w), 1034 (w), 1005 (w), 972 (w), 924 (m), 845 (w), 831 (w), 775 (w), 748 (m), 733 (m), 700 (s), 671 (m), 611 (m), 586 (w), 553 (w). Anal. Calcd for $C_{98}H_{90}B_2FeN_{10}O_{12}$: C, 70.18; H, 5.41; N, 8.35. Found: C, 70.75; H, 5.80; N, 7.64.

Synthesis of (*S*)-2·MeCN. The procedure is identical to that of **(*S*)-2·MeNO$_2$** except nitromethane was replaced acetonitrile in the recrystallized procedure. Dark violet block crystals (93 mg, 65%), suitable for X-ray crystallographic analysis, were obtained. ^{1}H NMR (600 MHz, CD_3CN): δ −3.2 (8 H), 3.3 (8 H) (Ph $H^{2/6}$+ $H^{3/5}$), 4.7 (4 H), 4.9 (4 H) (Ox H^3 and Ph H^4), 6.9 (8 H) ,7.1 (16 H), 7.4 (16 H) (BPh_4 H^4+$H^{3/5}$+$H^{2/6}$), 17.7 (4 H, Ox H^3), 25.2 (2 H, Py H^4), 30.2 (4 H, Ox H^4), 57.3 (4 H, Py $H^{3/5}$). FT-IR (KBr plate): ν 3676 (w), 3057 (w), 2985 (w), 2900 (w), 2162 (w), 1639 (w), 1618 (w), 1496 (w), 1479 (w), 1456 (w), 1425 (w), 1261 (w), 1201 (w), 1149 (w), 1076 (w), 1032 (w), 972 (w), 926 (w), 843 (w), 773 (w), 746 (w), 733 (w), 700 (w), 611 (w), 552 (w). Anal. Calcd for $C_{96}H_{81}B_2FeN_7O_4$: C, 78.21; H, 5.54; N, 6.65. Found: C, 77.28; H, 6.01; N, 6.12.

Synthesis of (*rac*)-2·3MeCN. The procedure is identical to that of **(*rac*)-2·MeNO$_2$** except nitromethane was replaced acetonitrile in the recrystallized procedure. Dark violet block crystals (93 mg, 67%), suitable for X-ray crystallographic analysis, were obtained. ^{1}H NMR (600 MHz, CD_3CN): δ 3.3 (8 H), 6.8 (8 H) (Ph $H^{2/6}$ + $H^{3/5}$), 4.5 (4 H), 6.2 (4 H), 7.2 (4 H), 7.5 (4 H) (Ox H^3 + H^4 and Ph H^4), 6.8 (8 H) ,7.0 (16 H), 7.3 (16 H) (BPh_4 H^4 + $H^{3/5}$ + $H^{2/6}$), 21.8 (2 H, Py H^4), 42.0 (4 H, Py $H^{3/5}$). FT-IR (KBr plate): ν 3676 (w), 3059 (w), 2987 (w), 2900 (w), 2186 (w), 1639 (w), 1620 (w), 1572 (w), 1554 (w), 1496 (w), 1481 (w), 1456 (w), 1396 (w), 1373 (w), 1288 (w), 1275 (w), 1250 (w), 1203 (w), 1138 (w), 1078 (w), 1034 (w), 1005 (w), 972 (w), 924 (w), 845 (w), 831 (w), 773 (w), 748 (w), 733 (w), 700 (w), 671 (w), 654 (w), 611 (w), 586 (w), 552 (w). Anal. Calcd for $C_{100}H_{87}B_2FeN_9O_4$: C, 77.18; H, 5.63; N, 8.10. Found: C, 76.28; H, 5.79; N, 7.57.

SI2.2 ^{1}H NMR spectra of Fe(II) complexes

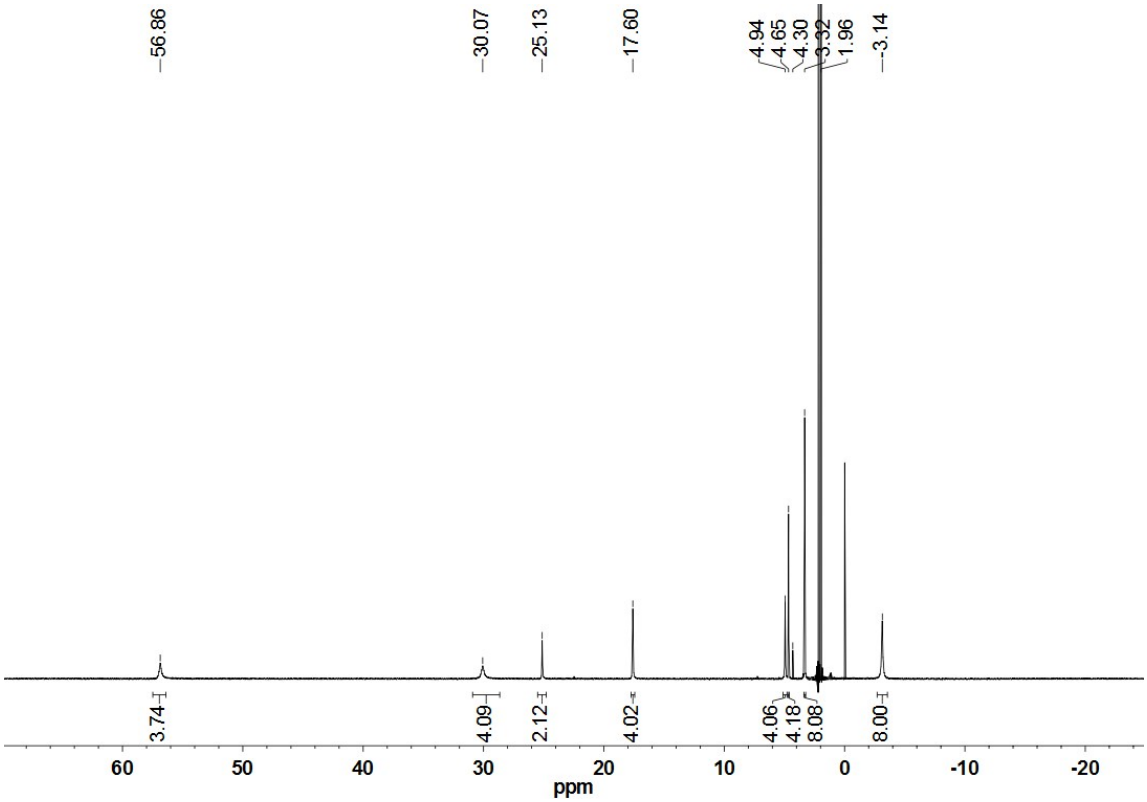

Fig. S1 Paramagnetic ^{1}H NMR spectra of **(*S*)-1·3MeCN** in CD_3CN.

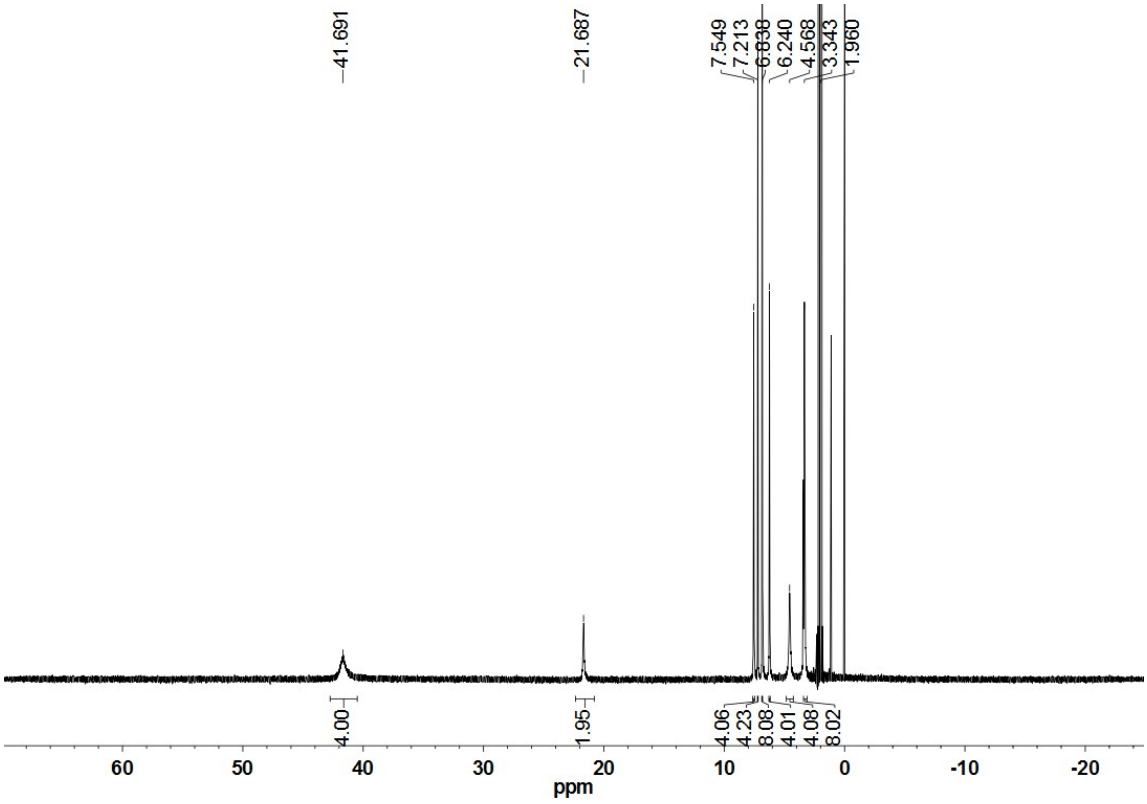

Fig. S2 Paramagnetic ^{1}H NMR spectra of **(*rac*)-1·3MeCN** in CD_3CN.

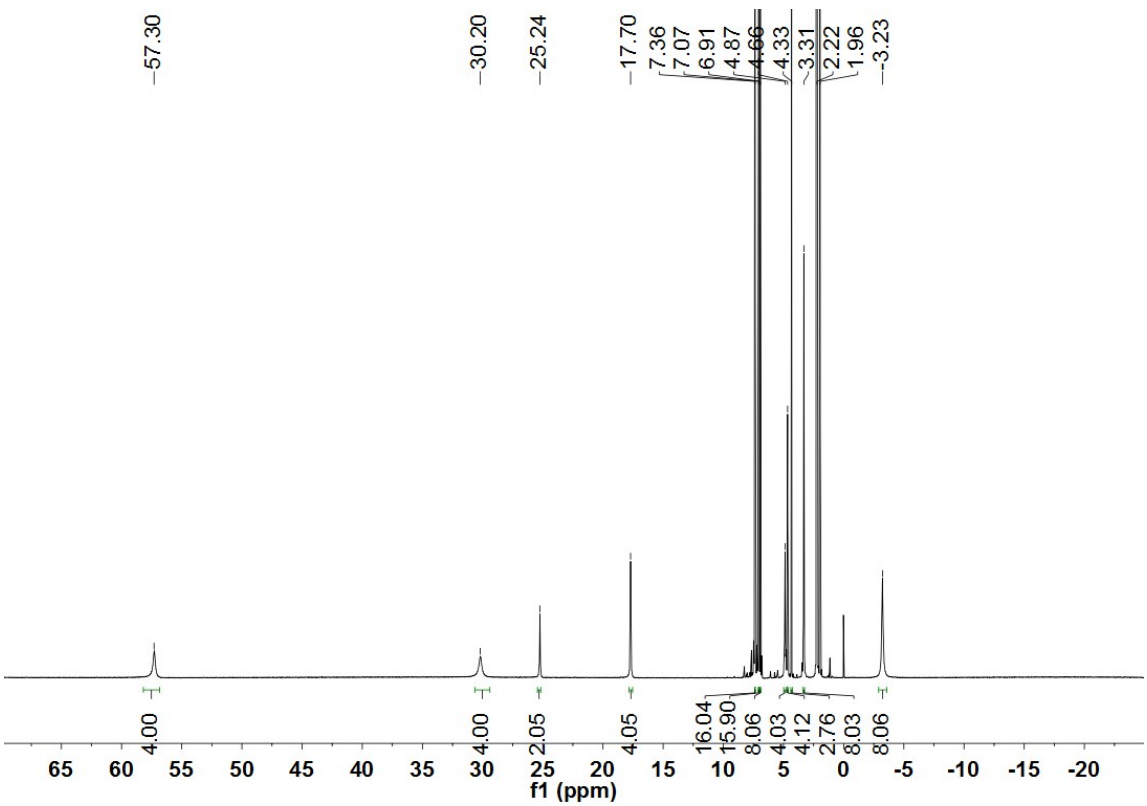

Fig. S3 Paramagnetic ^{1}H NMR spectra of **(*S*)-2·MeNO$_2$** in CD_3CN.

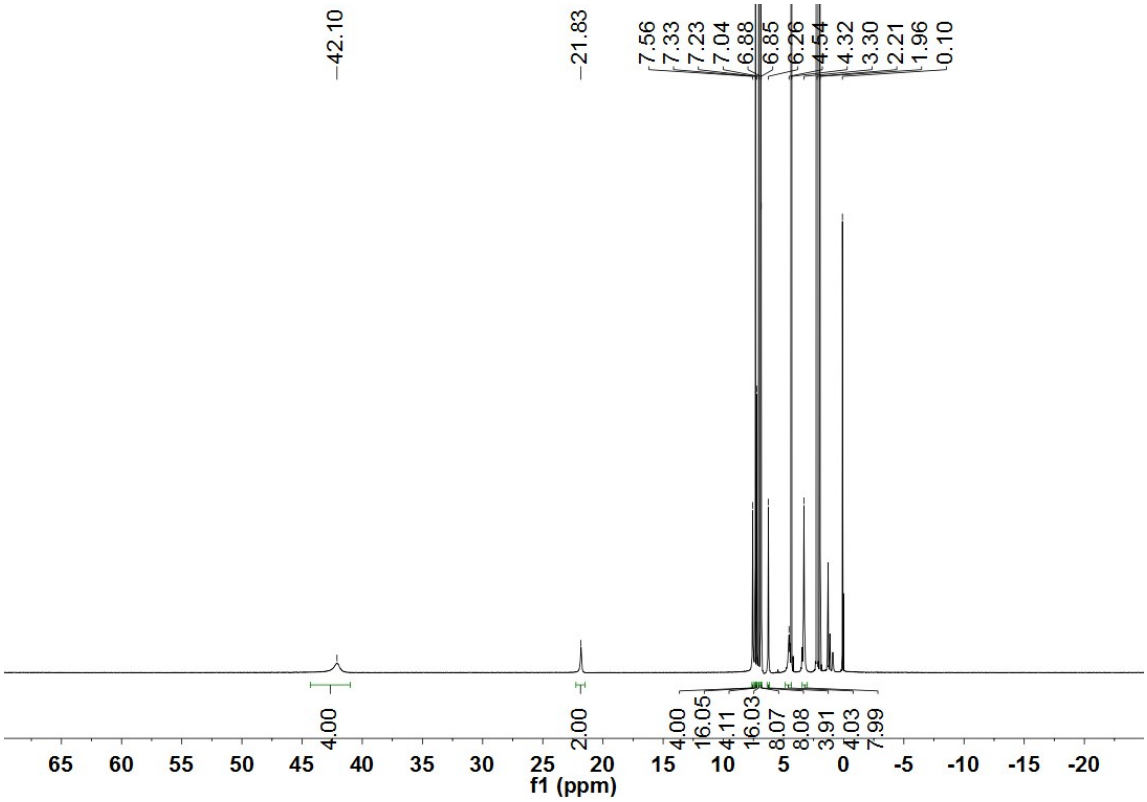

Fig. S4 Paramagnetic ^{1}H NMR spectra of **(*rac*)-2·4MeNO$_2$** in CD_3CN.

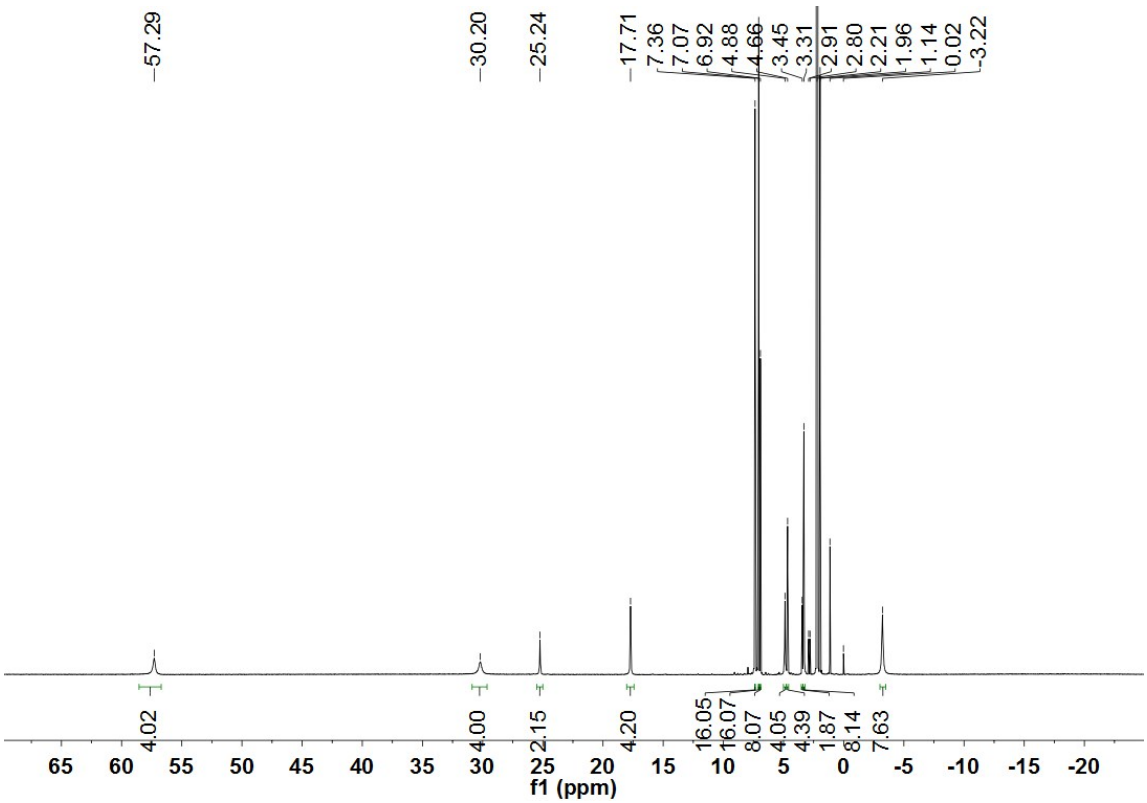

Fig. S5 Paramagnetic ^{1}H NMR spectra of **(*S*)-2·MeCN** in CD_3CN.

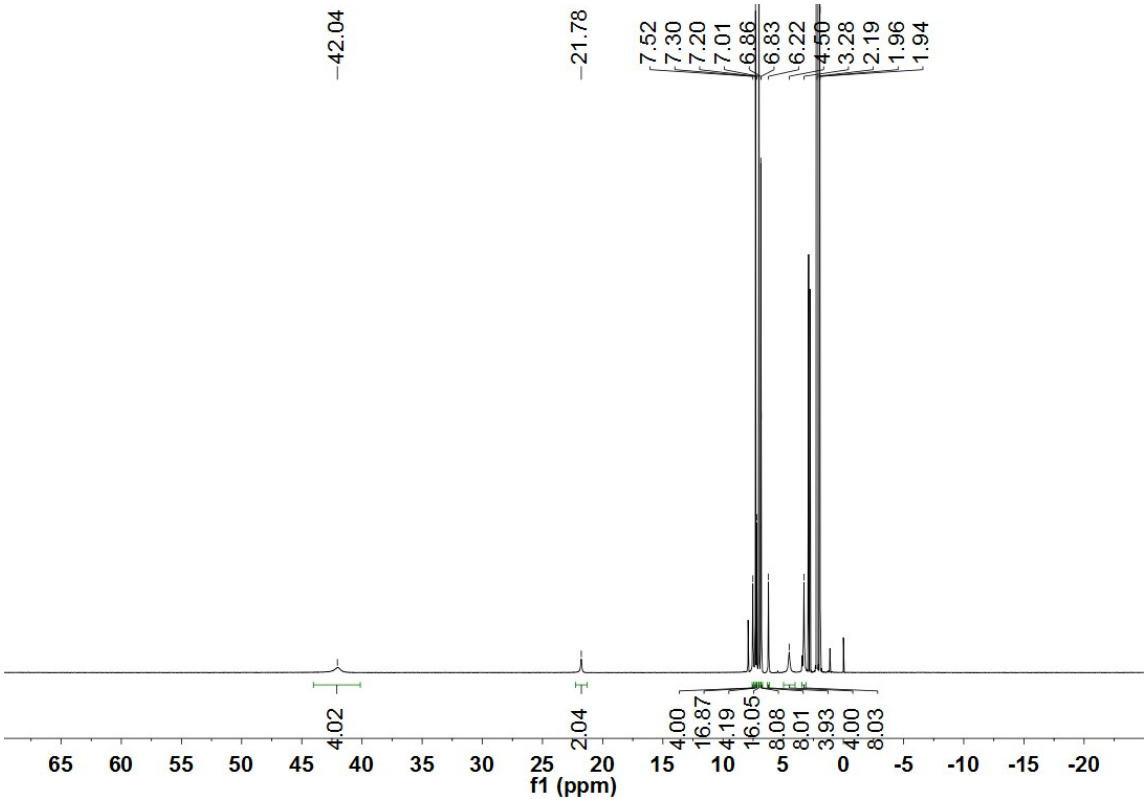

Fig. S6 Paramagnetic ^{1}H NMR spectra of **(*rac*)-2·3MeCN** in CD_3CN.

SI2.3 Structural characterization of Fe(II) complexes

Table S1. Crystal data, data collection, solution, and refinement information of iron(II) compounds in this work.

	(*S*)-**1**·3MeCN	(*S*)-**1**·3MeCN	(*rac*)-**1**·3MeCN	(*S*)-**2**·$MeNO_2$	(*rac*)-**2**·4$MeNO_2$	(*S*)-**2**·MeCN	(*rac*)-**2**·3MeCN
Formula	$C_{156}H_{141}N_{27}O_{36}Cl_6Fe_3$	$C_{104}H_{94}Cl_4Fe_2N_{18}O_{24}$	$C_{52}H_{47}Cl_2FeN_9O_{12}$	$C_{95}H_{81}B_2FeN_7O_6$	$C_{98}H_{90}B_2FeN_{10}O_{12}$	$C_{376}H_{312}B_8Fe_4N_{24}O_{16}$	$C_{100}H_{87}B_2FeN_9O_4$
formula weight	3350.20	2233.47	1116.73	1494.13	1677.26	5732.38	1556.25
crystal system	$P2_1$	$P2_12_12_1$	*P*bca	$P2_12_12_1$	*C*2/c	$P2_1$	$P\bar{1}$
space group	monoclinic	orthorhombic	orthorhombic	orthorhombic	monoclinic	monoclinic	triclinic
a, Å	19.120(4)	19.051(4)	20.660(4)	12.727(3)	22.871(5)	23.154(5)	13.388(3)
b, Å	21.609(4)	21.637(4)	21.568(4)	12.812(3)	14.773(3)	26.161(5)	13.558(3)
c, Å	21.015(4)	25.014(5)	22.524(5)	47.027(9)	27.221(5)	26.794(5)	26.002(5)
α, deg	90	90	90	90	90	90	78.99(3)
β, deg	116.91(3)	90	90	90	113.17(3)	97.46(3)	76.08(3)
γ, deg	90	90	90	90	90	90	65.62(3)
V, Å^3	7743(3)	10311(4)	10037(3)	7668(3)	8456(3)	16093(6)	4150.4(18)
Z	2	4	8	4	4	2	2
T, K	153.0(2)	173.0(2)	153.0(2)	153.0(2)	153.0(2)	153.0(2)	153.0(2)
F(000)	3468	4624	4624	3136	3520	6016	1636
D_C, g cm^{-3}	1.437	1.439	1.478	1.294	1.318	1.183	1.245
μ, mm^{-1}	0.468	0.469	0.481	0.260	0.249	0.243	0.242
λ, Å	0.71073	0.71073	0.71073	0.71073	0.71073	0.71073	0.71073
crystal size, mm^3	0.36 × 0.21 × 0.17	0.36 × 0.21 × 0.17	0.54 × 0.34 × 0.32	0.52 × 0.40 × 0.32	0.38 × 0.35 × 0.29	0.32 × 0.31 × 0.25	0.44 × 0.41 × 0.37
T_{min} and T_{max}	0.7102, 1.0000	0.9011, 1.0000	0.6590, 1.0000	0.7143, 1.0000	0.8151, 1.0000	0.7757, 1.0000	0.8071, 1.0000
θ_{min}, θ_{max}, deg	1.1943, 27.4855	1.2444, 27.4855	0.9040, 27.4816	1.6474, 27.4778	1.6275, 27.4816	1.3429, 27.4855	1.6225, 27.4855
no. total reflns.	66419	77662	30698	20573	28149	100918	48409
no. uniq. reflns, R_{int}	35105, 0.0402	23629, 0.0502	9119, 0.0718	15897, 0.0650	9674, 0.0466	52000, 0.0744	18804, 0.0560
no. obs. [$I \geq 2\sigma(I)$]	32438	22124	8361	12429	8951	39265	16896
no. params	1837	1375	688	1002	559	3853	1048
*R*1 [$I \geq 2\sigma(I)$]	0.0655	0.0613	0.0793	0.0914	0.0615	0.1052	0.0646
*wR*2 (all data)	0.1825	0.1580	0.1776	0.1589	0.1391	0.2467	0.1563
S	1.073	1.114	1.216	1.144	1.138	1.065	1.163
$\Delta\rho^a$, e/ Å^3	0.666, −0.919	0.745, −0.428	0.863, −0.383	0.430, −0.677	0.316, −0.355	0.400, −0.503	0.621, −0.592
max. and mean Δ/σ^b	0.000, 0.000	0.001, 0.000	0.001, 0.000	0.000, 0.000	0.001, 0.000	0.002, 0.000	0.001, 0.000
Flack parameter	−0.011(4)	0.023(6)	/	0.040(16)	/	0.046(15)	/
CCDC	1879551	1879552	1879553	1879554	1879555	1879557	1879556

Table S2. Selected bond lengths (Å) for **(*R*)-1·MeCN**, **(*rac*)-1·3MeCN**, **(*S*)-2·MeNO$_2$**, **(*rac*)-2·4MeNO$_2$**, **(*S*)-2·MeCN**, and **(*rac*)-2·3MeCN**.

(*S*)-1·3MeCN, Fe1		**(*S*)-1·3MeCN**, Fe2		**(*S*)-1·3MeCN**, Fe1		**(*S*)-1·3MeCN**, Fe2		**(*S*)-1·3MeCN**, Fe3		**(*rac*)-1·3MeCN**	
T / K	173 K	*T* / K	173 K	*T* / K	153 K	*T* / K	153 K	*T* / K	153 K	*T* / K	153 K
Fe1-N1	2.226	Fe2-N7	1.985	Fe1-N1	2.210	Fe2-N7	2.051	Fe3-N13	1.981	Fe1-N1	1.979(3)
Fe1-N2	2.128	Fe2-N8	1.901	Fe1-N2	2.105	Fe2-N8	1.984	Fe3-N14	1.907	Fe1-N2	1.907(3)
Fe1-N3	2.244	Fe2-N9	1.989	Fe1-N3	2.155	Fe2-N9	2.104	Fe3-N15	2.002	Fe1-N3	1.985(3)
Fe1-N4	2.173	Fe2-N10	1.998	Fe1-N4	2.279	Fe2-N10	1.964	Fe3-N16	2.011	Fe1-N4	1.987(3)
Fe1-N5	2.138	Fe2-N11	1.905	Fe1-N5	2.109	Fe2-N11	1.855	Fe3-N17	1.886	Fe1-N5	1.903(3)
Fe1-N6	2.182	Fe2-N12	1.999	Fe1-N6	2.186	Fe2-N12	2.080	Fe3-N18	2.022	Fe1-N6	1.976(4)

(*S*)-2·MeNO$_2$		**(*rac*)-2·4MeNO$_2$**	
T / K	153 K	*T* / K	153 K
Fe1-N1	2.188(11)	Fe1-N1	1.916(2)
Fe1-N2	2.105(11)	Fe1-N2	1.995(2)
Fe1-N3	2.224(11)	Fe1-N3	1.916(2)
Fe1-N4	2.169(11)	Fe1-N4	2.000(2)
Fe1-N5	2.133(11)		
Fe1-N6	2.170(11)		

(*S*)-2·MeCN, Fe1		**(*S*)-2·MeCN**, Fe2		**(*S*)-2·MeCN**, Fe3		**(*S*)-2·MeCN**, Fe4		**(*rac*)-2·3MeCN**	
T / K	153 K	*T* / K	153 K	*T* / K	153 K	*T* / K	153 K	*T* / K	153 K
Fe1-N1	2.205(6)	Fe2-N7	2.207(7)	Fe3-N13	2.153(6)	Fe4-N19	2.204(7)	Fe1-N1	2.188(11)
Fe1-N2	2.144(7)	Fe2-N8	2.144(7)	Fe3-N14	2.143(6)	Fe4-N20	2.157(6)	Fe1-N2	2.105(11)
Fe1-N3	2.213(6)	Fe2-N9	2.182(7)	Fe3-N15	2.164(6)	Fe4-N21	2.164(7)	Fe1-N3	2.224(11)
Fe1-N4	2.230(7)	Fe2-N10	2.239(7)	Fe3-N16	2.255(6)	Fe4-N22	2.229(7)	Fe1-N4	2.169(11)
Fe1-N5	2.127(7)	Fe2-N11	2.150(7)	Fe3-N17	2.112(7)	Fe4-N23	2.139(6)	Fe1-N5	2.133(11)
Fe1-N6	2.214(6)	Fe2-N12	2.247(6)	Fe3-N18	2.215(7)	Fe4-N24	2.253(7)	Fe1-N6	2.170(11)

Table S3. Summary of the structural parameters and spin state in the family of compounds reported in this work.

Entry	T (K)	Σ (°)	θ (°)	ϕ (°)	Fe–N_{av} (Å)	S (O_h)	Spin State
(*S*)-1·3MeCN, Fe1	153	154.4	82.4	179.4	2.174	5.553	HS
(*S*)-1·3MeCN, Fe2	153	112.9	86.6	177.0	2.006	2.297	LS
(*S*)-1·3MeCN, Fe3	153	101.3	85.3	178.0	1.968	5.426	LS
(*S*)-1·3MeCN, Fe1	173	155.3	82.9	176.5	2.182	3.354	HS
(*S*)-1·3MeCN, Fe2	173	97.2	86.2	179.3	1.963	2.379	LS
(*rac*)-1·3MeCN	153	92.0	89.5	178.1	1.956	2.315	LS
(*S*)-2·$MeNO_2$	153	162.9	80.7	167.7	2.165	6.233	HS
(*rac*)-2·4$MeNO_2$	153	95.4	90.0	180	1.957	2.463	LS
(*S*)-2·MeCN, Fe1	153	166.0	80.6	169.7	2.189	6.493	HS
(*S*)-2·MeCN, Fe2	153	169.5	78.9	167.3	2.195	6.553	HS
(*S*)-2·MeCN, Fe3	153	159.3	81.6	178.2	2.174	5.566	HS
(*S*)-2·MeCN, Fe4	153	165.7	80.9	166.7	2.191	6.593	HS
(*rac*)-2·3MeCN	153	143.7	86.9	177.6	2.165	5.119	HS

Σ: the sum of the deviations from 90° of the *cis* angles;[2] θ: the dihedral angle between the planes of the tridentate ligands; ϕ: the *trans*-N{pyridine}−Fe− N{pyridine} angle; Fe–N_{av}: the average value of the six Fe–N bond lengths in one FeN_6 coordination sphere; $S(O_h)$: the result of CShMs calculation denotes the deviation value of ideal O_h symmetry.[3]

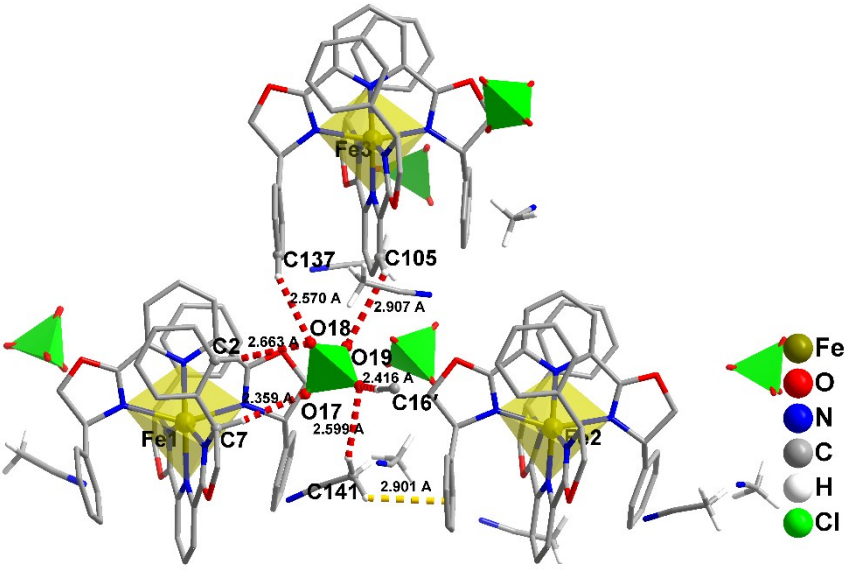

Fig. S7 Molecular structures of **(*S*)-1·3MeCN** at 153 K, the weak C–H···O hydrogen bonding between perchlorate anion and cationic complex/solvent is illustrated.

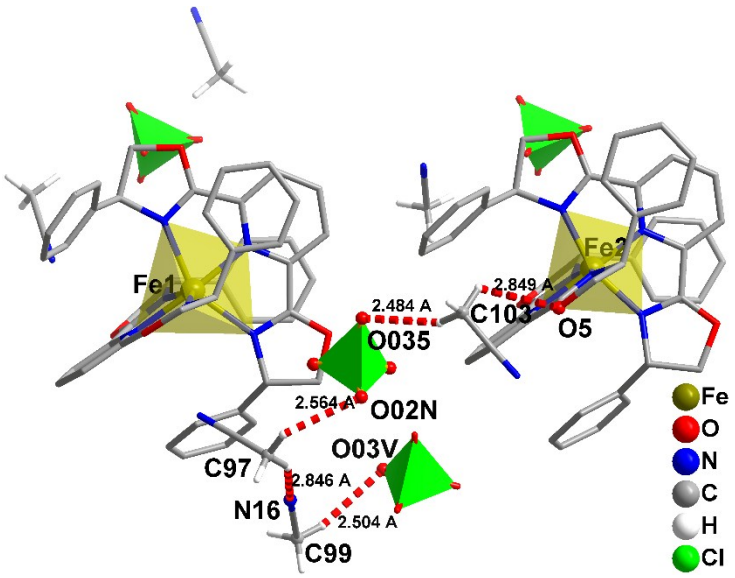

Fig. S8 Molecular structures of (a) **(*S*)-1·3MeCN** at 173 K, the weak C–H···O/N hydrogen bonding between perchlorate anion and cationic complex/solvent is illustrated.

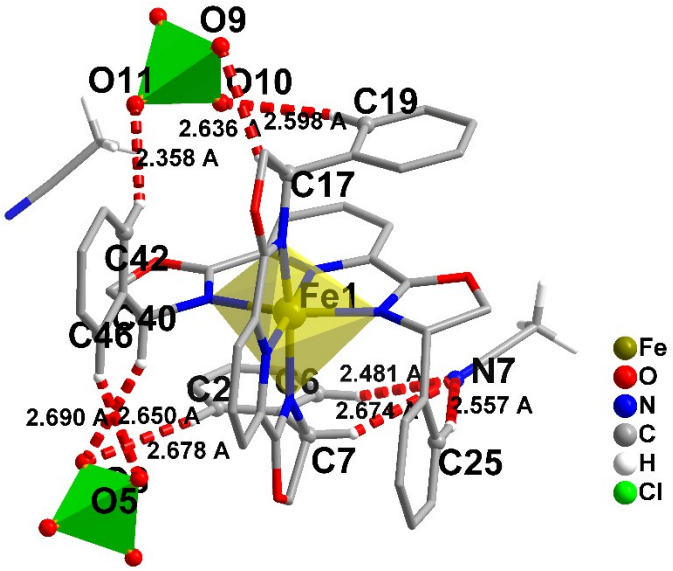

Fig. S9 Molecular structures of **(*rac*)-1·3MeCN** at 153 K, the weak C–H···O/N hydrogen bonding between perchlorate anion and cationic complex/solvent is illustrated.

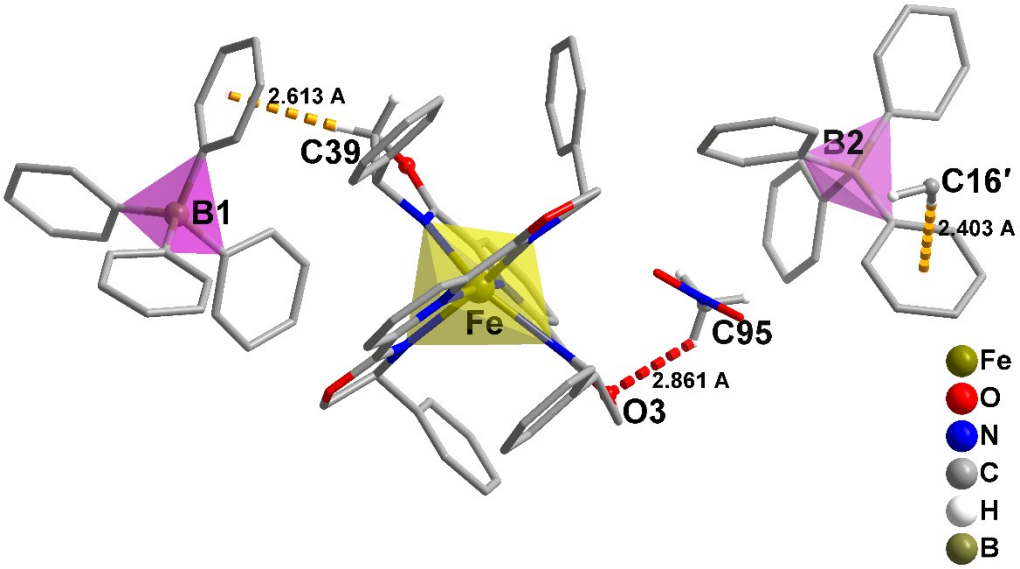

Fig. S10 Molecular structures of **(*S*)-2·MeNO$_2$**, the weak C–H···O hydrogen bonding between cationic complex and solvent and the weak C–H···π interaction between tetraphenylborate anion and cationic complex are illustrated.

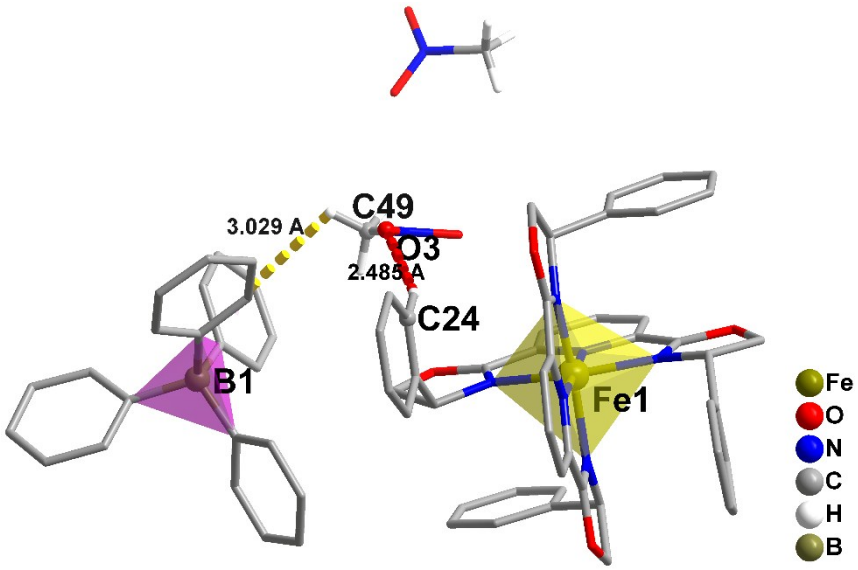

Fig. S11 Molecular structures of **(*rac*)-2·4MeNO$_2$**, the weak C–H···O hydrogen bonding between cationic complex and solvent and the weak C–H···π interaction between tetraphenylborate anion and solvent are illustrated.

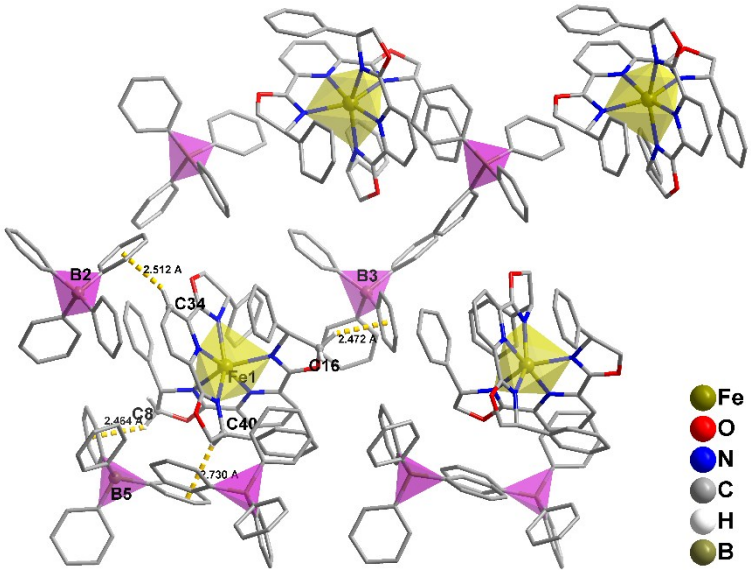

Fig. S12 Molecular structures of **(*S*)-2·MeCN,** the weak C–H···π interaction between tetraphenylborate anion and solvent is illustrated.

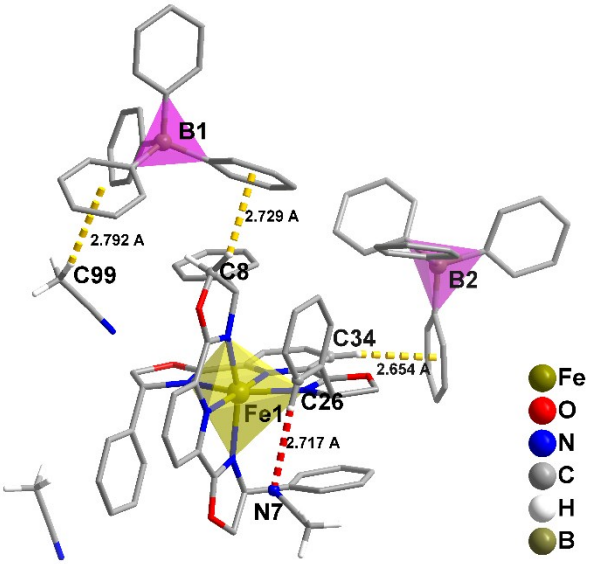

Fig. S13 Molecular structures of **(*rac*)-2·3MeCN**, the weak C–H···π interaction between tetraphenylborate anion and cationic complex/solvent is illustrated.

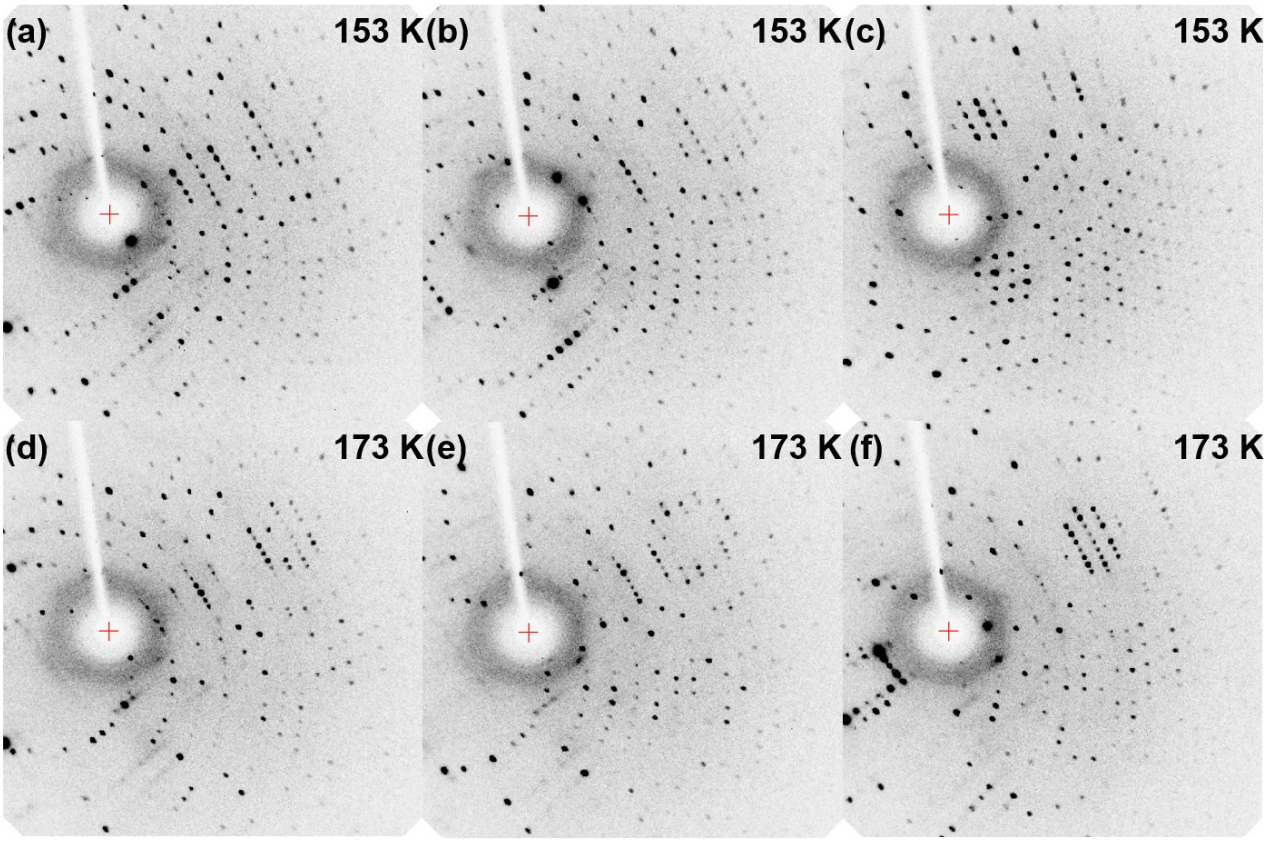

Fig. S14 The representative X-ray diffraction images of **(*S*)-1·MeCN** at 153 K (a-c) and at 173 K (d-f).

Table S4. Summary of dihedral angle between neighboring phenyl and pyridine in these Fe(II) complexes and their spin states.

Entry	T / *K*	**1**	**2**	**3**	**4**	Spin State
(*S*)-1·3MeCN, Fe1	173	4.517	1.405	30.116	30.561	HS
(*S*)-1·3MeCN, Fe1	173	6.857	6.010	17.976	18.083	LS
(*S*)-1·3MeCN, Fe1	153	5.051	1.197	27.616	30.490	HS
(*S*)-1·3MeCN, Fe2	153	3.080	5.700	26.166	20.415	LS
(*S*)-1·3MeCN, Fe3	153	5.535	5.284	17.668	18.549	LS
(*rac*)-1·3MeCN	153	3.593	4.143	6.809	9.150	LS
(*S*)-2·MeNO$_2$	153	4.689	6.076	9.011	53.375	HS
(*rac*)-2·4MeNO$_2$	153	3.040	3.040	6.781	6.781	LS
(*S*)-2·MeCN, Fe1	153	10.678	12.618	14.871	53.485	HS
(*S*)-2·MeCN, Fe2	153	1.349	17.275	20.063	48.761	HS
(*S*)-2·MeCN, Fe3	153	2.702	7.171	25.456	41.507	HS
(*S*)-2·MeCN, Fe4	153	10.660	13.841	14.653	68.256	HS
(*rac*)-2·3MeCN	153	2.628	3.384	4.068	4.363	HS

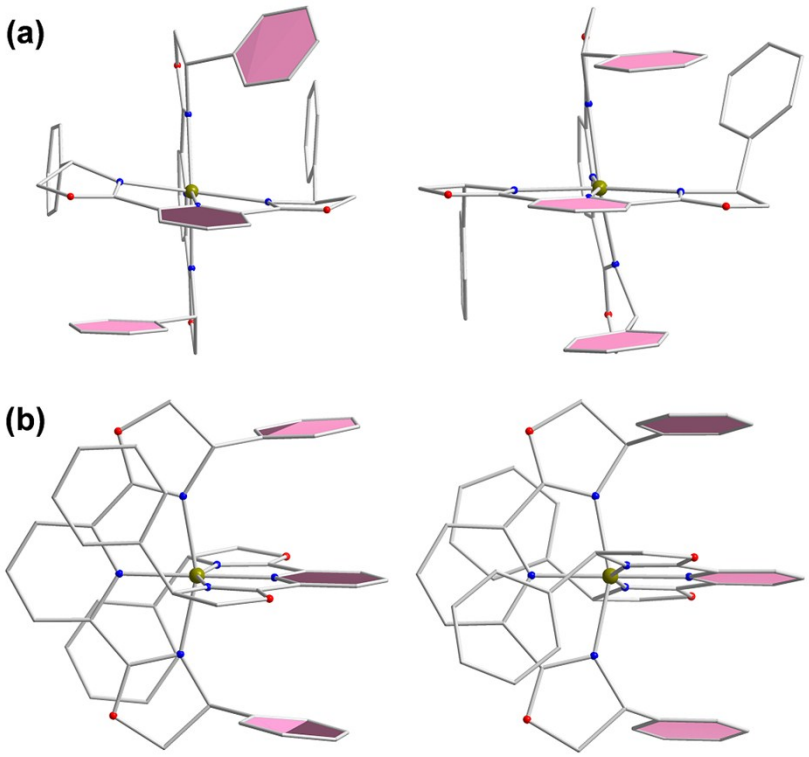

Fig. S15 The illustration of dihedral angle between neighboring phenyl and pyridine in these Fe(II) complexes, (a) homochiral series and (b) heterochiral series.

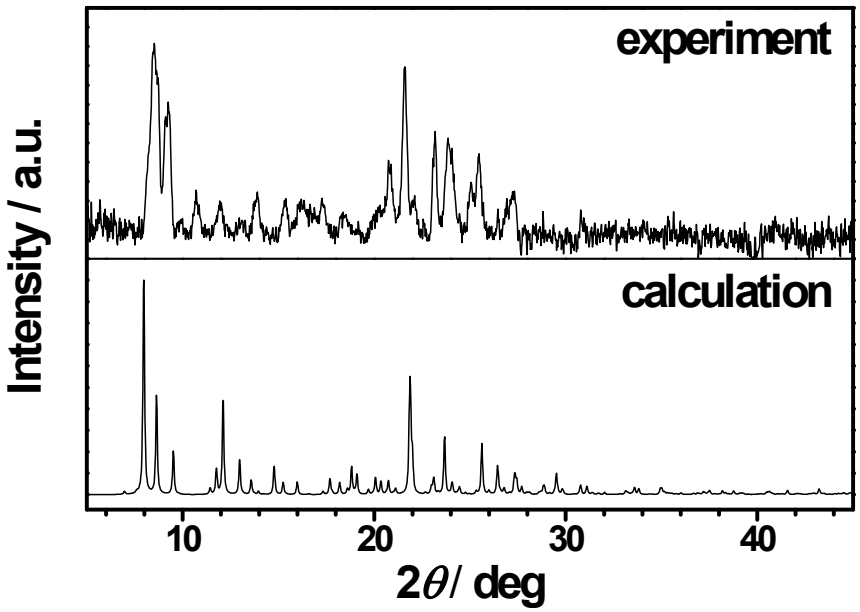

Fig. S16 The powder XRD pattern of **(*S*)-1·3MeCN** and the simulated pattern from the single-crystal X-ray structure.

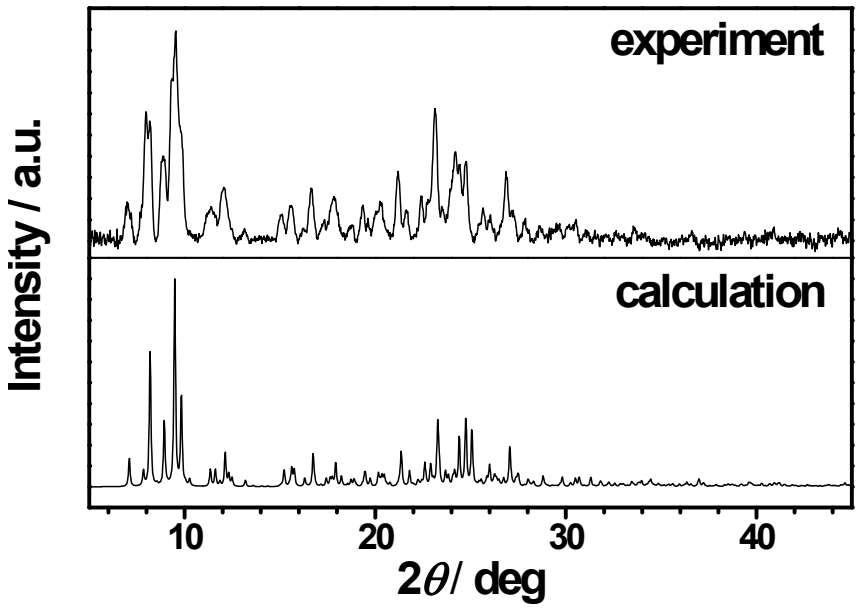

Fig. S17 The powder XRD pattern of **(*rac*)-1·3MeCN** and the simulated pattern from the single-crystal X-ray structure.

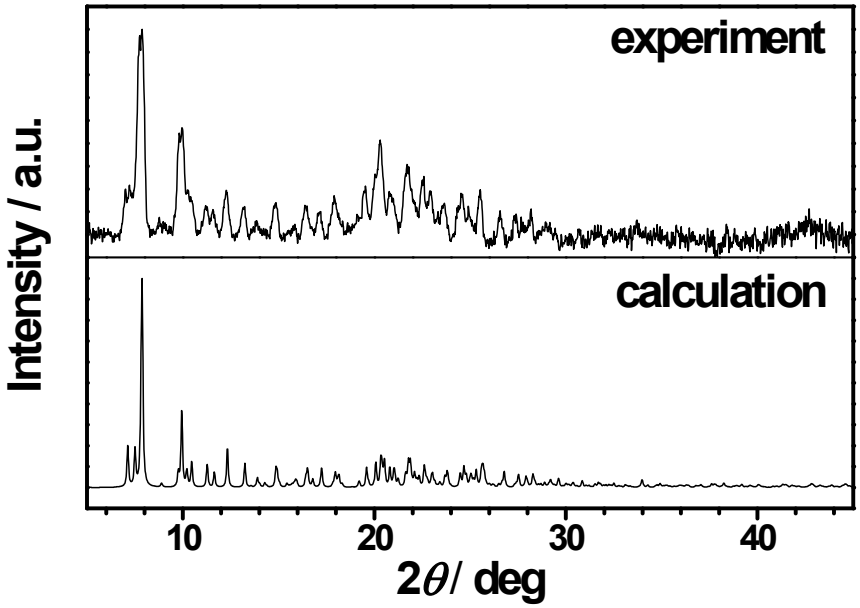

Fig. S18 The powder XRD pattern of **(*S*)-2·MeNO$_2$** and the simulated pattern from the single-crystal X-ray structure.

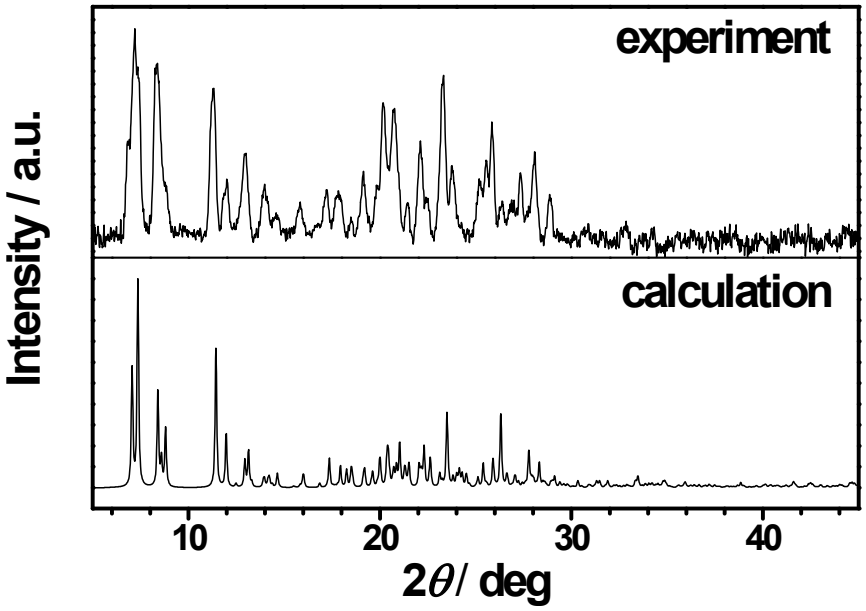

Fig. S19 The powder XRD pattern of **(*rac*)-2·4MeNO$_2$** and the simulated pattern from the single-crystal X-ray structure.

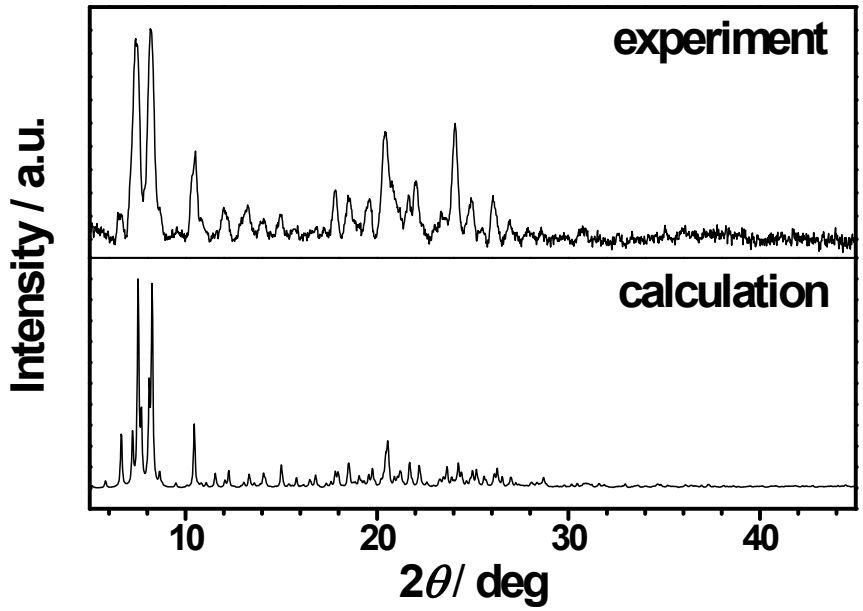

Fig. S20 The powder XRD pattern of **(*S*)-2·MeCN** and the simulated pattern from the single-crystal X-ray structure.

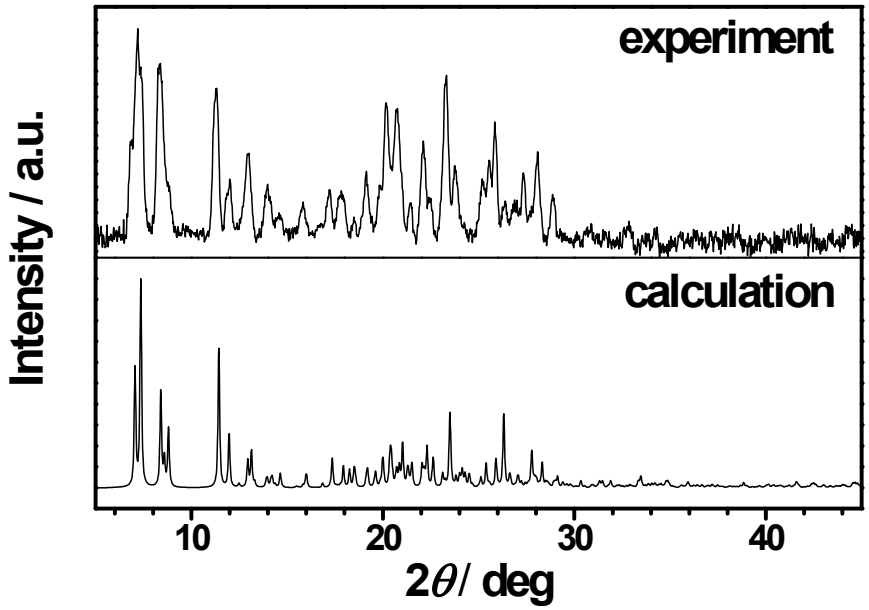

Fig. S21 The powder XRD pattern of **(*rac*)-2·3MeCN** and the simulated pattern from the single-crystal X-ray structure.

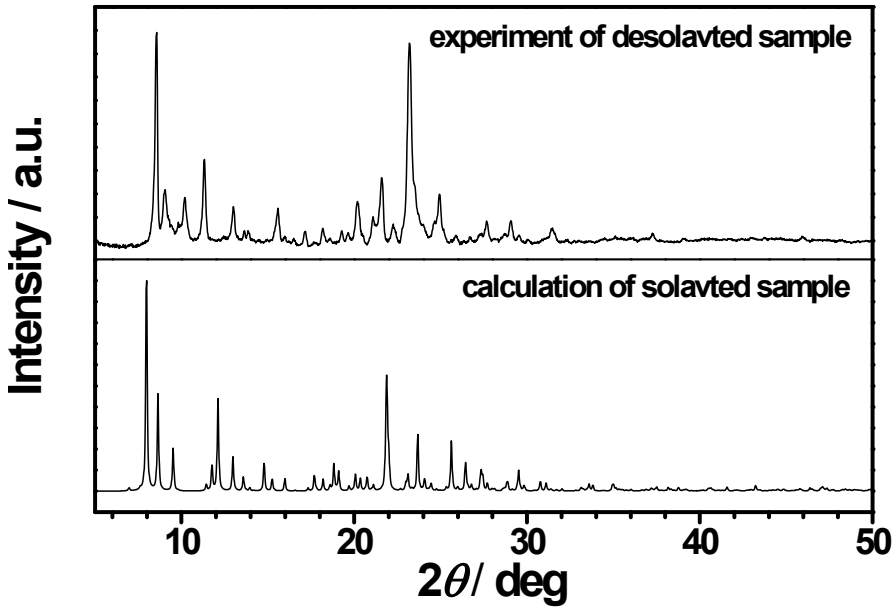

Fig. S22 The powder XRD pattern of desolvated **(*S*)-1·3MeCN** and the simulated pattern from the single-crystal X-ray structure of solvated sample.

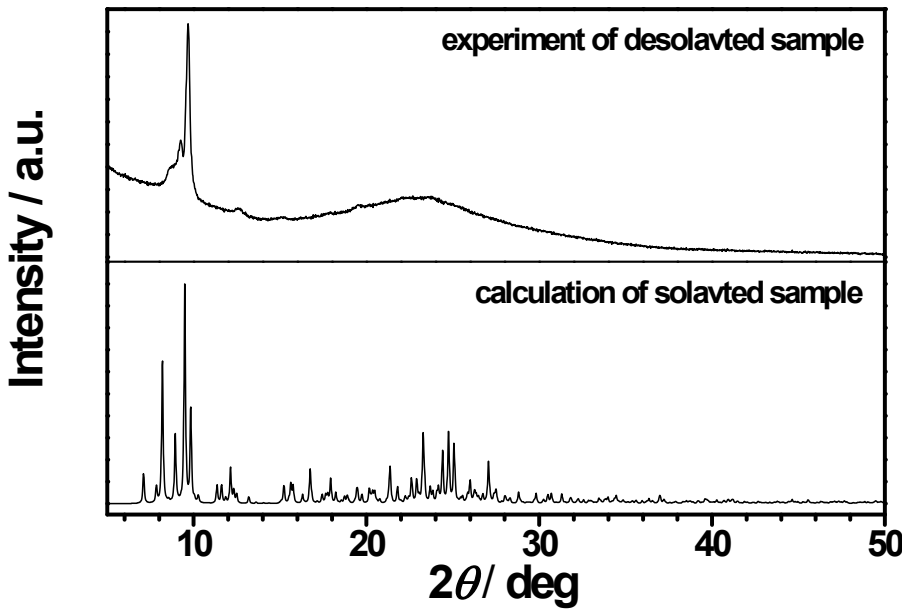

Fig. S23 The powder XRD pattern of desolvated **(*rac*)-1·3MeCN** and the simulated pattern from the single-crystal X-ray structure, indicating the partial loss of crystallinity after desolvation of solvent at 400 K for 4 hours.

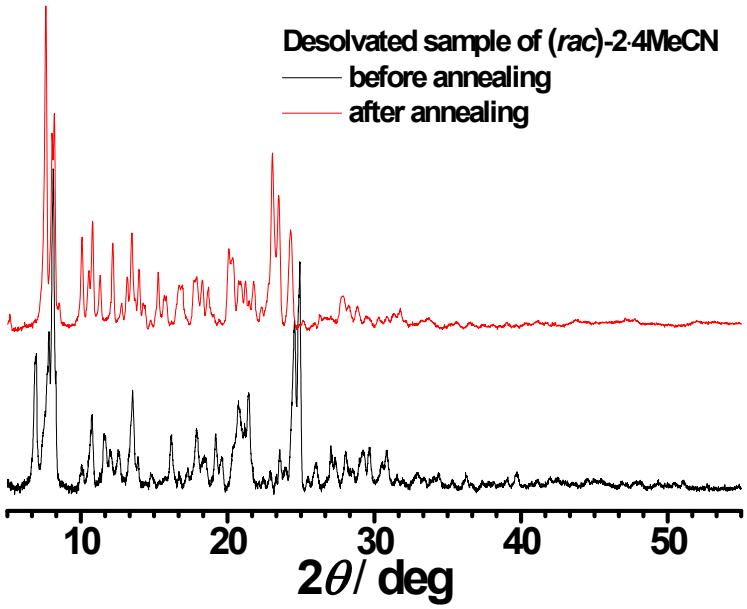

Fig. S24 Powder XRD pattern of desolvated **(*rac*)-2·3MeCN** before (black) and after (red) annealing at 400 K.

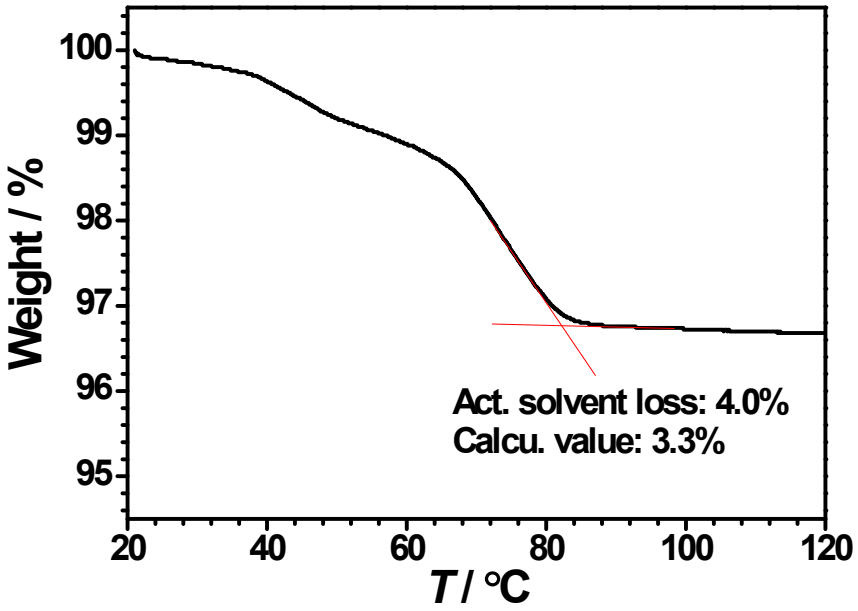

Fig. S25 The TGA trace of **(*S*)-1·MeCN**, indicating the loss of acetonitrile completes below 100 °C. To avoid the explosion of perchloride compound at higher temperature, the heating was ceased at 120 °C.

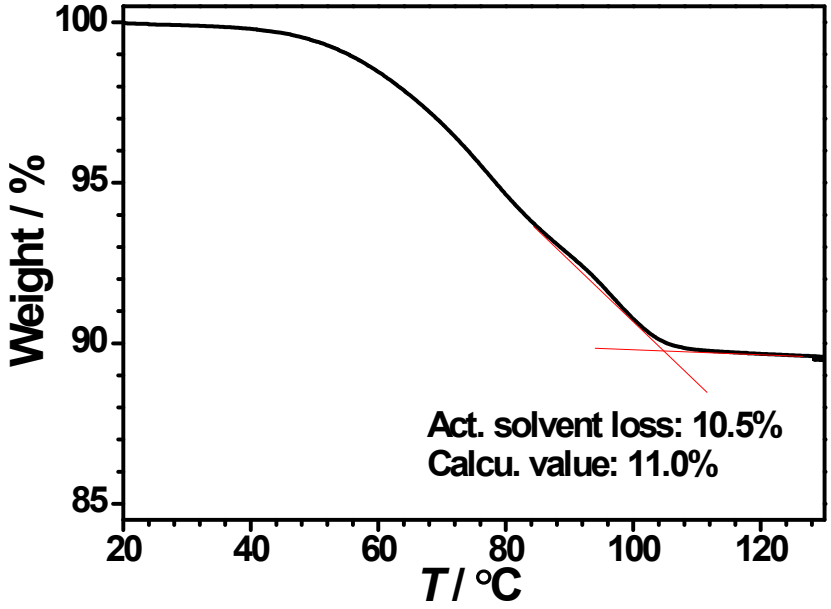

Fig. S26 The TGA trace of **(*rac*)-1·3MeCN**, indicating the loss of acetonitrile completes below 100 °C. To avoid the explosion of perchloride compound at higher temperature, the heating was ceased at 120 °C.

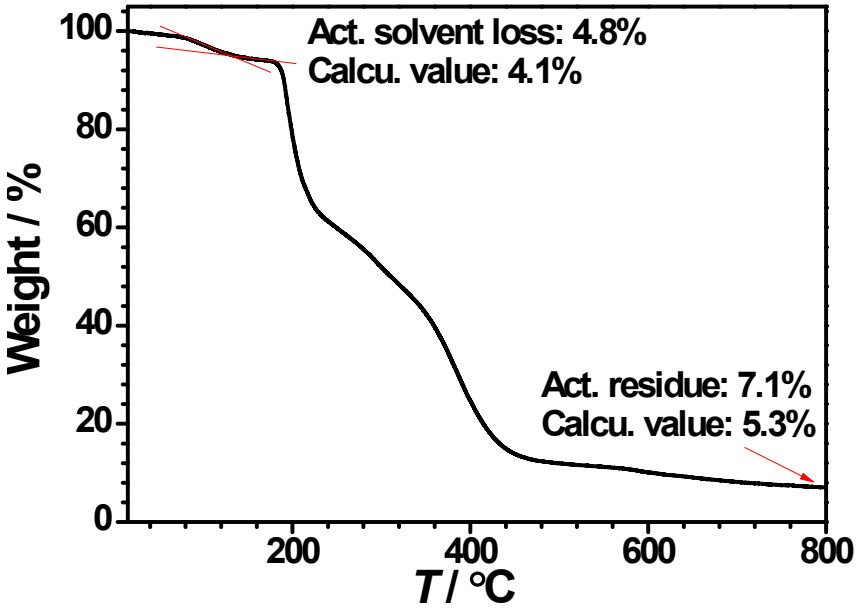

Fig. S27 The TGA trace of **(*S*)-2·MeNO$_2$**, indicating the loss of nitromethane completes below 140 °C.

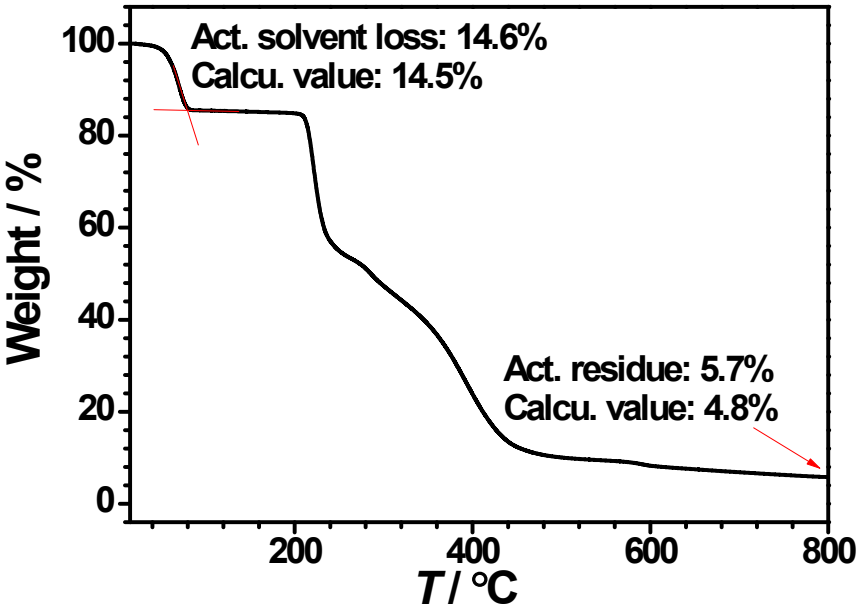

Fig. S28 The TGA trace of **(*rac*)-2·4MeNO$_2$**, indicating the loss of nitromethane completes below 100 °C.

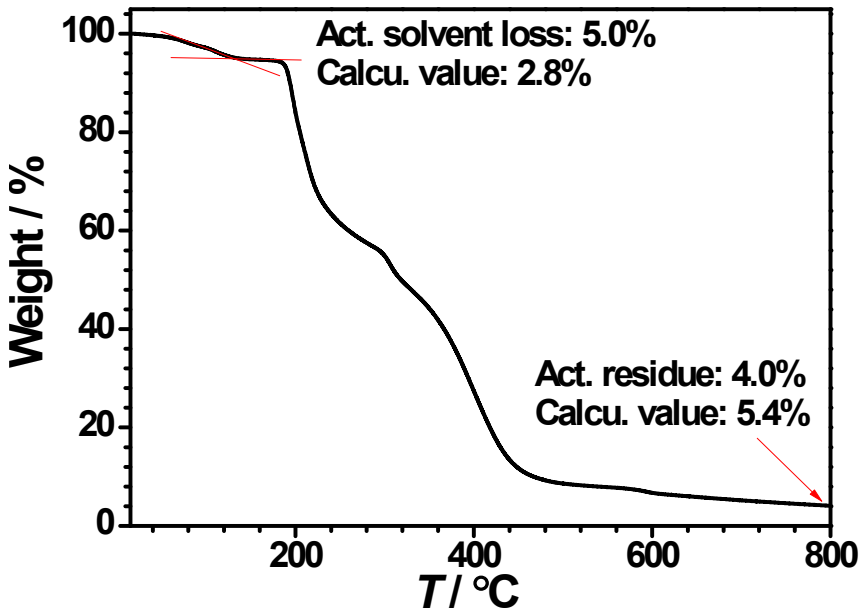

Fig. S29 The TGA trace of **(*S*)-2·MeCN**, indicating the loss of acetonitrile completes below 140 °C.

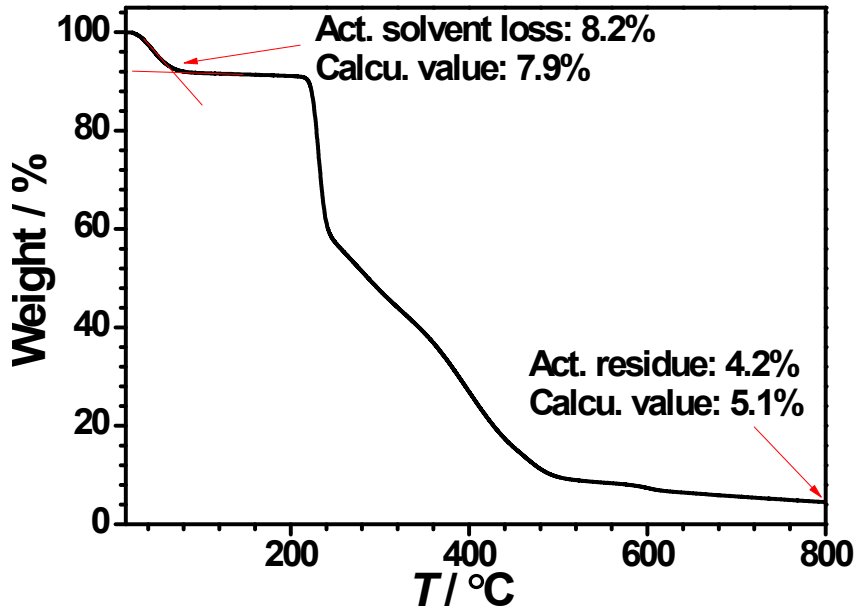

Fig. S30 The TGA trace of **(*rac*)-2·3MeCN**, indicating the loss of acetonitrile completes below 100 °C.

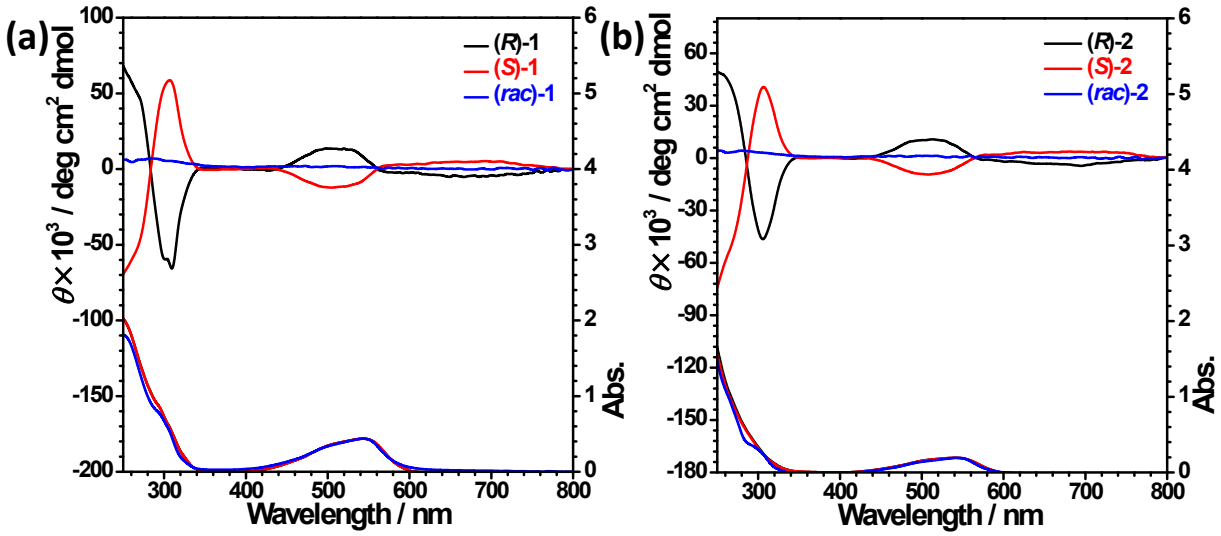

Fig. S31 CD and UV-vis spectra of (a) **(*R or S*)-1** and **(*rac*)-1** and (b) **(*R or S*)-2** and **(*rac*)-2** with the concentration of 1.0×10^{-4} M in chloroform.

SI3 Supplementary magnetic data

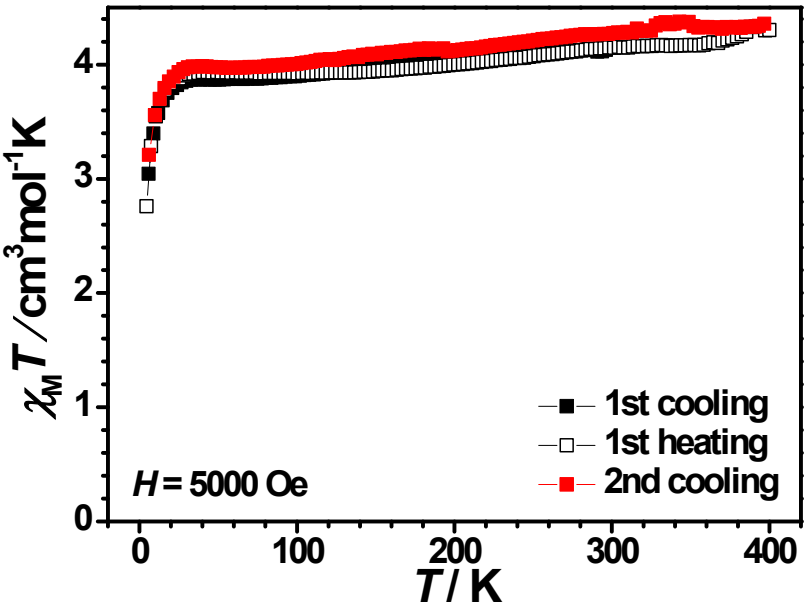

Fig. S32 Temperature variations of the $\chi_M T$ products for **(*S*)-2·MeNO$_2$**.

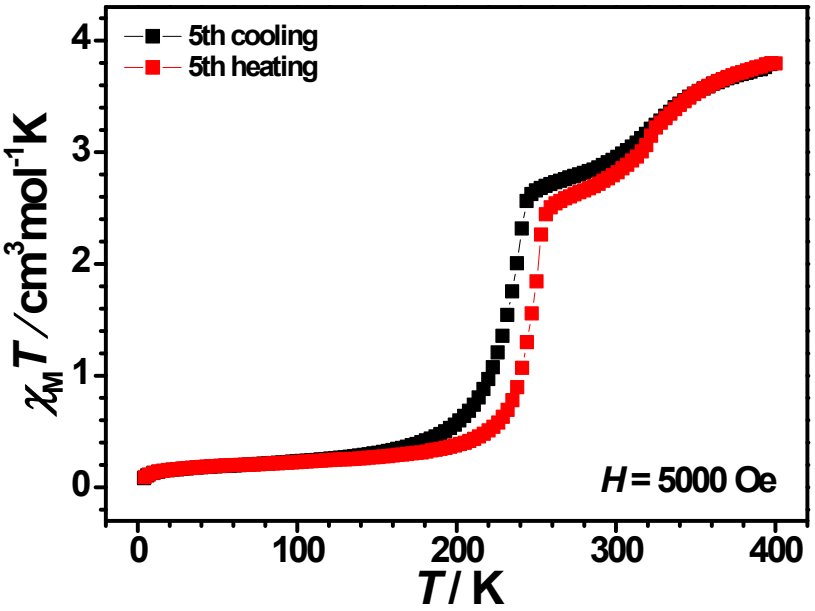

Fig. S33 Temperature variations of the $\chi_M T$ products for **(*rac*)-2·4MeNO$_2$** in the 5th cycle.

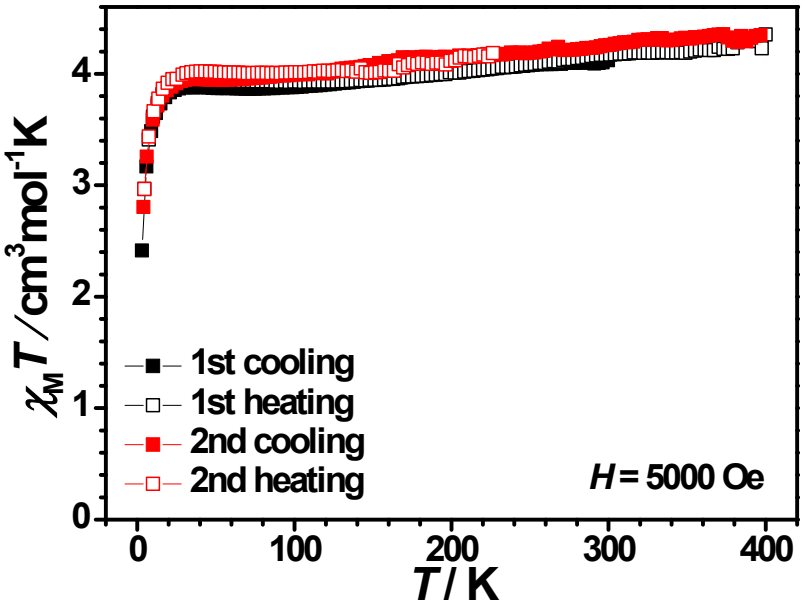

Fig. S34 Temperature variations of the $\chi_M T$ products for **(*S*)-2·MeCN**.

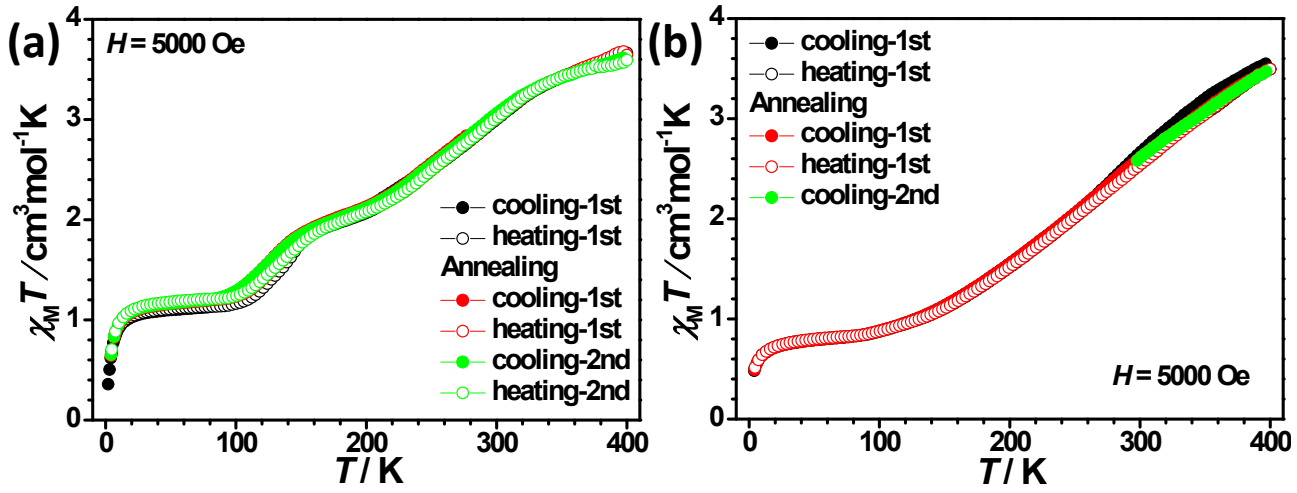

Fig. S35 Temperature variations of the $\chi_M T$ products for desolvated **(*S*)-1·3MeCN** (a) and **(*rac*)-1·3MeCN** (b) before and after annealing at 400 K for 4 hours.

SI4 References

1. Y.-Y. Zhu, C. Cui, N. Li, B.-W. Wang, Z.-M. Wang and S. Gao, *Eur. J. Inorg. Chem.*, 2013, **2013**, 3101-3111.
2. P. Guionneau, M. Marchivie, G. Bravic, J. F. Létard and D. Chasseau, *Top. Curr. Chem.*, 2004, **234**, 785-786.
3. M. Llunell, D. Casanova, J. Cirera, P. Alemany and S. Alvarez, *SHAPE, version 2.0,* , 2010, Universitat de Barcelona, Barcelona, Spain.